OPEN ACCESS

Study of the Electrochemical and Self-healing Processes of Galinstan as an Anode Material for Li-ion Batteries

To cite this article: Florent Mohimont *et al* 2023 *J. Electrochem. Soc.* **170** 050535

Journal of The Electrochemical Society, 2023 **170** 050535

Study of the Electrochemical and Self-healing Processes of Galinstan as an Anode Material for Li-ion Batteries

Florent Mohimont, Ronan Le Ruyet,[z] Reza Younesi, and Andrew J. Naylor

Department of Chemistry - Ångström Laboratory, Uppsala University, 75121 Uppsala, Sweden

Alloy electrodes are attracting a lot of interest in the field of Li-ion batteries due to their high energy density. However, they suffer from large volume expansion and contraction during lithiation and delithiation, leading to rapid pulverization and disconnection. A strategy to avoid this is to use self-healing materials. Ga-based liquid alloys have been studied as self-healing electrodes because of their capacity to store Li and their liquid state at room temperature. The so-called "galinstan" ($Ga_{0.77}In_{0.15}Sn_{0.08}$) exhibits the lowest melting temperatures and has also been used to add self-healing properties in composite electrodes. Nevertheless, its lithiation mechanism and its practical capacity still remain unknown. Also, the reversibility of the lithiation, which is crucial to ensure the self-healing properties offered by the liquid metal, requires investigation. In this work, electrochemical measurements were coupled with XRD and SEM analyses to better understand the redox processes, structural and morphological properties of galinstan as an electrode material in Li-ion batteries. It was shown that only Ga and In would react with Li to form LiGa and LiIn. The reversibility of these reactions and thus the self-healing ability of galinstan was demonstrated through observation of its liquid state before and after electrochemical cycling.

 [DOI: 10.1149/1945-7111/acd420]

Manuscript submitted December 29, 2022; revised manuscript received April 23, 2023. Published May 25, 2023.

Supplementary material for this article is available online

The growing demand of electronic devices and electric vehicles requires the development of batteries that are more efficient and that can store more energy in a smaller volume and weight. Li-ion batteries are currently the highest performing batteries found on the market because of their unmatched combination of high energy and power density. As a result, and due to the large range of chemistries available, they are used in numerous applications.[1] However, further improvements are required such as higher energy density, longer lifetime performance and improved safety factors.[2] One way to do so is to replace the traditional graphite anode (specific capacity of 374 $mAh.g^{-1}$) by other materials that offer higher capacity and other properties for improved cell performance. Alloying anodes are promising alternatives because of their relatively high specific capacity, e.g. 3579 $mAh.g^{-1}$ for silicon. However, such materials generally suffer from poor cycle life due to the extreme volume expansion and contraction upon cycling, which results in fracturing and fragmentation of the electrode.[3] An alternative is gallium-based liquid metals because of their self-healing properties and relatively high capacities. For instance, Guo et al. have used the eutectic Ga-In alloy, composed of 78.2 wt% of Ga and 21.8 wt% of In and having a melting temperature of 15 °C, as an anode material.[4] By supporting the liquid metal nanoparticles with carbon black and a binder, they prepared an electrode that could heal from its cracking and that had no delamination. During lithiation, the alloy solidifies and expands in volume. During delithiation it decreases in volume. However, at the end of the delithiation, the alloy becomes liquid again and self-heals the surface defects.[4] Wu et al. used a Ga-Sn liquid alloy made of 88 wt% of Ga and 12 wt% of Sn. This alloy has a melting point of 20 °C but is capable of super-cooling to −6 °C.[5] By using nanoparticles of the metal alloy stabilized in a reduced graphene oxide/carbon nanotube skeleton, nearly 100% of the capacity could be retained after 4000 cycles.[5] Some groups have used Ga-In-Sn (galinstan) liquid alloy to form nano-composites made of nanoparticles of silicon and galinstan.[6–9] The liquid alloy is used to "heal" the cracking in the silicon electrode by filling the cracks due to its liquid nature and to ensure electrical contact of the electrode with the current collector.[8] Another application of galinstan is to use it as a liquid metal coating on current collectors to induce epitaxial lithium plating.[10] The current collector is covered with galinstan and when lithium is plated on it, lithium ions can diffuse on the surface of the liquid metal thus avoiding plating at a fixed site and forming dendrites, it results in the epitaxial growth of Li.[10] However, the lithiation mechanism of these alloys is still unclear. Thus it is difficult to estimate the effect of such alloys on the capacity of the electrode or to know if the lithiation reaction is fully reversible to the pristine liquid state. These are the aspects that are focused on in this study, investigating galinstan as the alloy with the lowest melting temperature expected from the alloys based on Ga, In and Sn.

The term "galinstan" is a portmanteau of the words: gallium, indium and stannum (latin for tin). Even though its composition can slightly vary in the examples found in the literature, its eutectic point is often described to be at 67 wt% gallium, 20.5 wt% indium and 12.5 wt% tin (77 at. % gallium, 15 at. % indium and 8 at. % tin), with a melting temperature of 10.5 °C.[11–14] Each individual constituent metal of galinstan has previously been demonstrated as an alloying electrode for Li-ion batteries. Gallium alloys with lithium to form Li_2Ga upon full lithiation, delivering a theoretical capacity of 769 $mAh.g^{-1}$.[15–18] The lithiation mechanism of gallium involves three reactions occurring at 0.8 V, 0.6 V and ~ 0 V to form respectively Li_2Ga_7, LiGa and Li_2Ga.[15,17,19,20] Indium alloys with lithium to form four different phases: $Li_{0.3}In_{1.7}$, LiIn, Li_5In_4 and Li_3In_2. The capacity for the formation of Li_3In_2 is 351 $mAh.g^{-1}$.[21] Finally, tin alloys in seven steps to form: Li_2Sn_5, LiSn, Li_7Sn_3, Li_5Sn_2, $Li_{13}Sn_5$, Li_7Sn_2 and $Li_{22}Sn_5$.[22–25] The theoretical capacity for the formation of $Li_{22}Sn_5$ is 993 $mAh.g^{-1}$.[22,26] Based on the assumption that all of the constituant elements of galinstan would become fully lithiated, a theoretical capacity of 711 $mAh.g^{-1}$ was calculated. This number was obtained by normalizing the maximum theoretical capacity of each individual element by their weight fraction in galinstan. The few studies using galinstan as an electrode material for Li-ion batteries show that it alloys with Li but none have attempted to explain quantitatively nor qualitatively how its lithiation mechanism occurs.[6–8,10,27]

In this work, the electrochemical mechanism involved in the lithiation/de-lithiation of galinstan is studied by combining galvanostatic cycling, cyclic voltammetry and X-ray diffraction (XRD). Furthermore, the morphology of the alloy before and after lithiation is observed by scanning electron microscopy (SEM).

Experimental

Galinstan preparation.—The galinstan alloy was prepared with the following proportions: 67 wt% Ga (Sigma Aldrich, 99.99%),

[z]E-mail: ronan.leruyet@kemi.uu.se

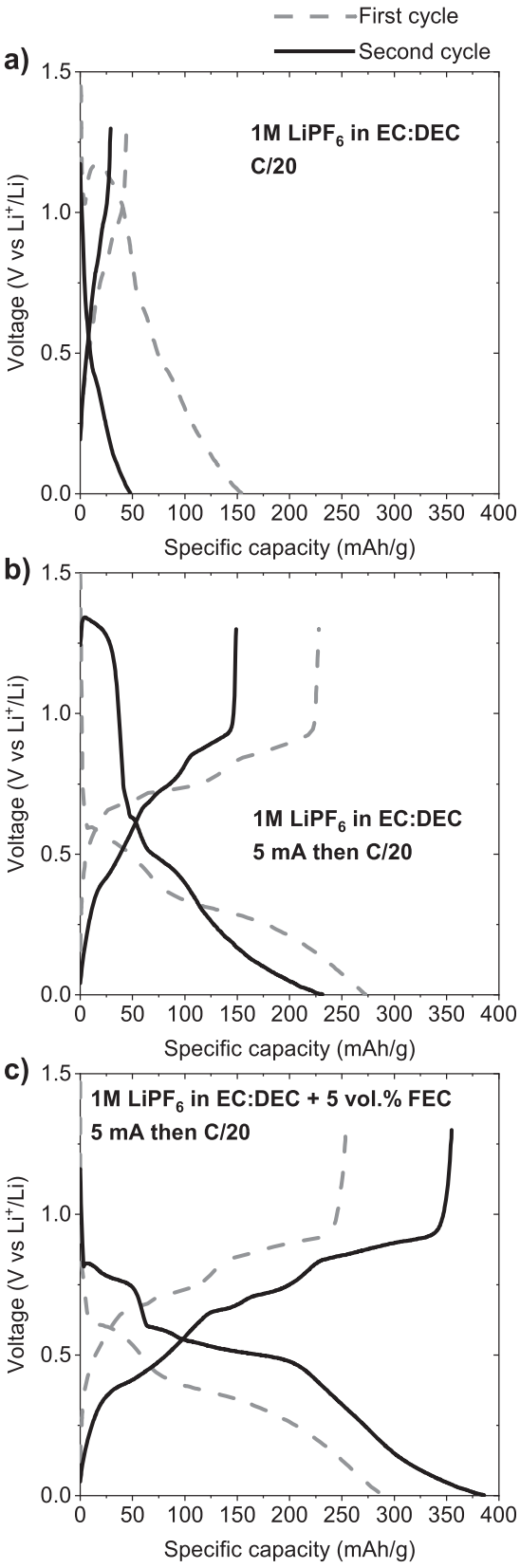

Figure 1. Galvanostatic cycling of (a) a half-cell using galinstan:C (90:10) working electrode and Li as counter and reference electrode. The electrolyte used was 1 M $LiPF_6$ in EC:DEC (1:1 volume ratio). The cell was cycled at C/20 (~1 mA) between 0.001 and 1.3 V. (b) the same cell configuration and composition but with a first discharge at 5 mA. (c) the same cell configuration also cycled with a first discharge at 5 mA but with 5 wt% of FEC added to the electrolyte.

20.5 wt% In (Good Fellow, 99.999%), 12.5 wt% Sn (Sigma Aldrich, 99.8%). The three metals were heated at 150 °C for 1 h in a glass vial on a hot plate in an argon-filled glove box (<1 ppm of O_2 and <1 ppm of H_2O, inner temperature ~30 °C).

Electrode preparation.—The electrodes were made with a mass ratio of active material:conductive additive of 90:10. They were prepared in an argon-filled glovebox (<1 ppm of O_2 and < 1 ppm of H_2O, inner temperature ~30 °C) by mixing 900 mg of galinstan with 100 mg of carbon black (Imerys, super C65), in 4 ml of acetonitrile (Sigma Aldrich, anhydrous, 99.8%) containing 4 mg of sodium docetyl sulfate (SDS, Sigma Aldrich, 99%) as a surfactant. The mixture was dispersed using an air tight ZrO_2 ball milling jar with 25 balls (powder:balls mass ratio = 1:10), shaken twice at 30 Hz for 30 min using a Retsch shaker. Finally, the excess of acetonitrile was removed with a syringe and the remaining acetonitrile was evaporated under vacuum until a fine homogeneous powder could be recovered.

Electrolyte preparation.—Two electrolytes were used, 1 M $LiPF_6$ in EC:DEC 1:1 volume ratio (LP40, Solvionic) with and without 5 vol.% of FEC (fluoroethylene carbonate, Solvionic, 99.9%). The electrolytes were handled in an argon filled glovebox (<1 ppm of O_2 and <1 ppm of H_2O, inner temperature ~30 °C).

Cell assembly.—Swagelok half-cells were assembled in an argon-filled glovebox (<1 ppm of O_2 and <1 ppm of H_2O, inner temperature ~30 °C). The Swagelok parts are made of stainless steel and the inner part is insulated using a polyethylene film. The diameter of the plungers that are used as current collectors is 12.8 mm. The cells were assembled by first pouring 20 ± 1 mg of the electrode powder into the cell. Then, two glass fiber separators (Whatman, glass fiber filters) of diameter 13 mm were placed on top of the powder. The Li electrodes were cut from a foil. The Li electrode was placed on the separators and a copper current collector was added on the top of it. Finally, a spring was placed on the top of the stack to maintain a constant pressure during cycling. The electrolyte was added last to the cell; the volume used per cell was 150 μl. The swagelok cells were sealed in the glovebox and taken out for electrochemical cycling.

Scanning electron microscopy (SEM) and energy dispersive X-ray spectroscopy (EDS).—Scanning electron microscopy imaging was done with a Zeiss LEO 1530 microscope. An electron acceleration voltage of 20 kV was used. The sample was prepared by spreading a small amount of the electrode powder on a sample holder covered with carbon tape.

Energy dispersive X-ray spectroscopy was performed in the SEM using an Oxford Instruments AZtec system and the AZtec (INCA energy) software for X-ray mapping and elemental analysis.

Electrochemical cycling.—Land potentiostats were used to perform galvanostatic cycling. All the cells were cycled at approximately 22 °C with cut-off potentials of 0.001 and 1.3 V vs Li^+/Li. Applying a negative current to the cell is referred to as discharge (lithiation of galinstan) and the opposite is referred to as charge (delithiation of galinstan) in this work. The C-rate was calculated based on the theoretical capacity of 711 $mAh.g^{-1}$ described in the introduction. A period of 12 h rest was applied before starting the measurements to ensure a good wetting of the electrodes with the electrolyte and to reach equilibrium at the electrode/electrolyte interfaces.

Cyclic voltammetry was performed using an MPG potentiostat from BioLogic and with the same half-cell set-up as for galvanostatic measurements. The initial scan started at the open circuit voltage (OCV, ~ 2.5 V vs Li^+/Li) and continued towards reducing potentials until a vertex voltage of 0.001 V vs Li^+/Li. It was then switched towards oxidizing potentials to a vertex voltage of 1.5 V vs Li^+/Li. The scan rate was 0.01 mV s^{-1}.

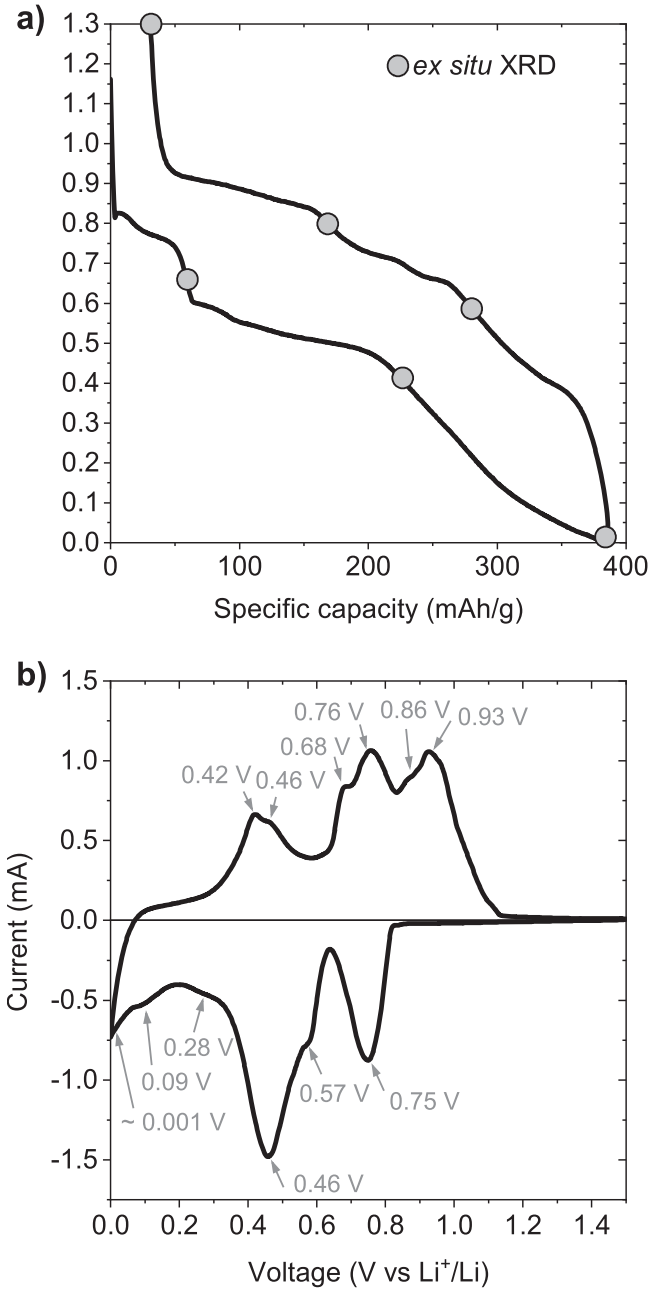

Figure 2. (a) Second galvanostatic cycle of a half-cell using galinstan+C (90:10) working electrode and Li as counter and reference electrode. The electrolyte used was 1 M $LiPF_6$ in EC:DEC (1:1 volume ratio) with 5 wt% of FEC. The cell was cycled at C/20 between 0.001 and 1.3 V with a first cycle at 5 mA. The grey spots represent where cells used for ex situ XRD were stopped (see Fig. 3). (b) Second cycle of the cyclic voltammogram of a cell with the same configuration and composition, with a scan rate of 0.01 mV s^{-1} and voltage limits of 0.001 and 1.5 V.

Ex situ powder X-ray diffraction (PXRD).—Ex situ powder X-ray diffraction was performed on electrode powders before and after galvanostatic cycling at different states of charge. The electrode powder was recovered from the Swagelok cells in an argon-filled glovebox (<1 ppm of O_2 and <1 ppm of H_2O, inner temperature ~30 °C). The powder was first cleaned with 300 μl of DEC to remove the $LiPF_6$ salt from the electrode so it would not appear on the diffractogram. The DEC was then removed with a syringe and the powder dried under vacuum at room temperature for 5 min The powder was placed in a borosilicate glass capillary with 0.6 mm inner diameter and walls with 0.01 mm thickness. Due to the air sensitivity of these samples, the capillaries were filled in the Argon filled glovebox and sealed using epoxy resin. XRD measurements were performed in transmission using a Stoe diffractometer in the Debye–Scherrer configuration. The acquisition was made with a duration of 1 h in the range of 5° to 115° 2θ. The patterns were analyzed with the Topas software from Bruker.

Results and Discussion

Cells with galinstan anodes were cycled galvanostatically at C/20 vs Li metal with 1 M $LiPF_6$ in EC:DEC (Fig. 1a). An anomalous irreversible capacity is observed during the first discharge at ~1.2 V. This irreversible capacity has been described in the literature for indium[28] and tin[29] but not for galinstan and is believed to be a decomposition of the electrolyte due to a catalytic activity of the active material. This phenomenon is still not very well understood. Beattie et al. assumed it was due to the catalytic activity of pure tin,[29] whereas Webb et al. suggested that it was due to the catalytic activity of indium oxide.[28] It was assumed this decomposition of the electrolyte forms a passivation layer that hinders the diffusion of lithium ions to the electrode, which results in a low capacity, particularly for the subsequent cycles.[29]

To overcome this issue, Beattie et al. proposed to apply a higher current during the first discharge until the potential reaches the first lithiation plateau, around 0.8 V and perform the subsequent cycles at C/20.[29] In Fig. 1b, the result of the cycling after using a higher current of 5 mA for the first discharge is shown. No anomalous plateau is observed during the first cycle and the capacity is significantly improved. However, the anomalous plateau reappears during the second cycle. FEC was added to the electrolyte following the observation of Webb et al. who showed that the use of FEC as an electrolyte additive can improve the cycling of indium vs lithium.[28] The use of an higher current for the first discharge with the addition of 5 wt% of FEC in the electrolyte gives the greatest improvement, as shown in Fig. 1c. No anomalous irreversible capacity appears at 1.2 V, the capacity is improved and the plateaus are well-defined.

The galvanostatic curve from the second cycle of this cell is replotted in Fig. 2a to enable easier observation of the different plateaus and their possible reversibility. On discharge, a first short plateau appears at approximately 0.8 V. It is preceded by a small voltage drop which is often observed at the beginning of alloying reactions. Then a longer plateau appears at approximately 0.6 V. The discharge ends with a long slope similar to what can be observed during the lithiation of gallium and tin.[15,22] For instance, in the case of gallium, the slope corresponds to the formation a of a Li_xGa solid solution, with x = 1 to 1.3, as described by Saint et al.[19] The subsequent charge starts with a plateau at 0.40 V, after which several plateaus appear at approximately 0.7 V and 0.9 V. A clear separation of the different plateaus could not be achieved, even using the derivative plot (dQ/dV, see Fig. S1), so cyclic voltammetry measurements were also performed to help to distinguish the potentials at which the different reactions happen (Fig. 2b). The second cycle of the cyclic voltammetry is shown, to provide the greatest comparability to the galvanostatic curve. On reduction, six reactions appear at 0.75, 0.57, 0.46, 0.28, 0.09 and 0.001 V. These potentials are slightly different from those observed for the galvanostatic cycling, especially at low potentials. The slope below 0.50 V observed by the galvanostatic measurement seems to be due to at least three reactions as observed on the cyclic voltammogram. Six reactions also appear on oxidation at 0.42, 0.46, 0.68, 0.76, 0.86 and 0.93 V. Due to the complexity of the results obtained by galvanostatic cycling and cyclic voltammetry, XRD analysis was required for further interpretation.

Ex situ XRD analysis was performed to identify the compounds formed during the lithiation of galinstan (see Fig. 3). Samples were cycled to different potentials, on discharge and charge, corresponding to the end of the main plateaus observed during the galvanostatic cycling of galinstan (Fig. 2a).

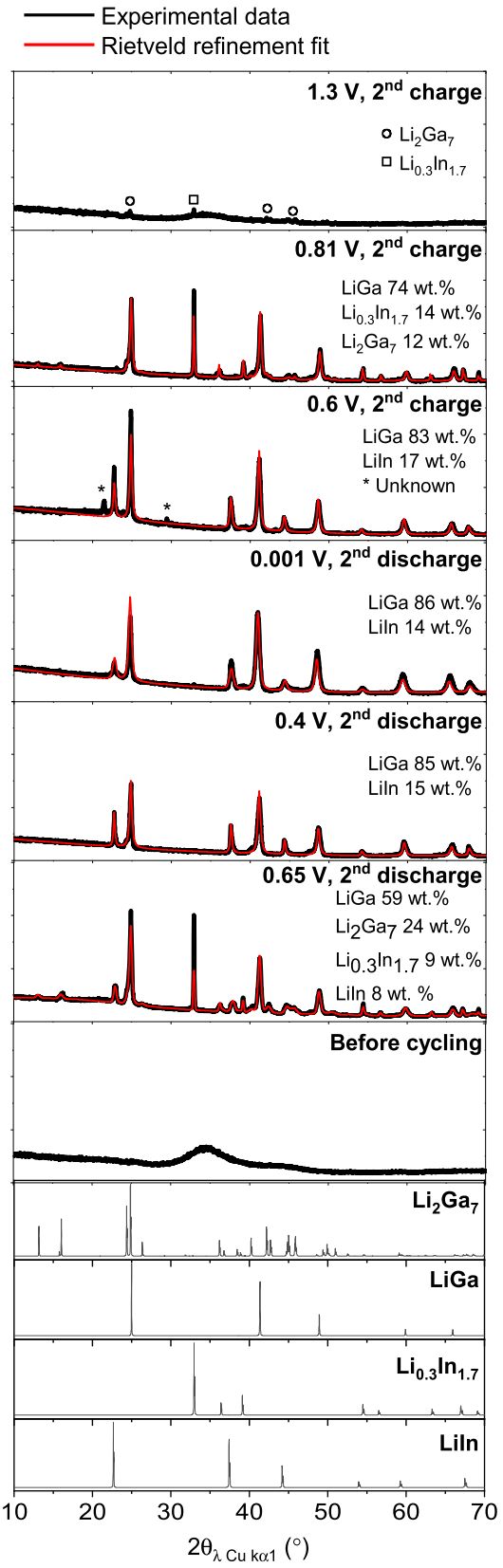

Figure 3. Ex situ XRD patterns of galinstan+C (90:10) electrodes, cycled to different potential points, from half-cells using galinstan+C (90:10) working electrodes and Li as counter and reference electrode. The electrolyte used was 1 M $LiPF_6$ in EC:DEC (1:1 volume ratio) with 5 wt% of FEC. The cells were cycled at C/20 between 0.001 and 1.3 V with a first discharge at 5 mA. The ex situ diffractograms are compared to the theoretical patterns of the compounds formed during the cycling.

The first measurement was taken before cycling and the diffractogram shows two very broad peaks between 30° and 50°. It shows that the alloy is amorphous, with an ordered structure only on small distances, similar to the diffractogram of liquid gallium.[30] Galinstan seems to be a solid solution with the structure of Ga, with partial substitution by In and Sn atoms. At 0.65 V during the discharge, Li_2Ga_7, LiGa, $Li_{0.3}In_{1.7}$ and LiIn are observed. Then, at 0.4 V and the end of discharge (0.001 V) only LiGa and LiIn are observed. The same observation is made during the charge at 0.6 V. At 0.81 V, all of the LiIn turns into $Li_{0.3}In_{1.7}$ and part of LiGa turns into Li_2Ga_7. At the end of the charge, at 1.3 V, the liquid alloy reappears. Only very small peaks of Li_2Ga_7 and $Li_{0.3}In_{1.7}$ are observed. It can be noted that no Sn or Li_xSn compounds are observed.

From ex situ XRD, it is observed that the compounds formed at the end of the lithiation step are LiGa and LiIn. The theoretical capacity obtained for the formation of these two compounds from the lithiation of galinstan is 345 $mAh.g^{-1}$. This value is close to the one observed with the galvanostatic measurement (386 $mAh.g^{-1}$). The slight difference could be explained by the formation of more lithiated phases such as Li_5In_4, Li_3In_2 and Li_2Ga but in too small amount to be observed by XRD and to significantly increase the capacity. Neither gallium nor indium are completely lithiated at the end of the discharge. This seems to be due to an excessive cell polarization, resulting in the decrease of the voltages needed to further lithiate these compounds. For instance, the potential of the LiGa to Li_2Ga plateau is very low (~0.02 V), so any cell polarization can prevent further lithiation after the formation of LiGa.[15,19] An attempt to link the different potentials of reaction with the formation and decomposition of various Li_xGa and Li_xIn compounds was made, as summarized in Table I. It was done by comparing the species observed by XRD at different states of charge with the observed potentials obtained by cyclic voltammetry measurements. It should be noted that even though it gives some insight into the mechanisms of lithiation and delithiation of galinstan, this assignment was intricate to perform based on the obtained data and still raises some issues. First, no evidence for the formation of Li_xSn species could be found. It could be because tin represents only 12.5 wt% of the alloy, making the detection of its lithiation more difficult. Furthermore, since broad peaks are usually obtained on the XRD pattern of fully lithiated tin, such peaks would likely not be visible in the XRD pattern of lithiated galinstan.[31] Nevertheless, the values of capacity seem to indicate that tin might not be active in this alloy. Li et al. also observed that tin does not react with Li in the case of the Ga-Sn eutectic liquid alloy (weight percent of tin = 8%).[32] Secondly, not every reaction could be attributed to a potential due to peak overlaps in cyclic voltammetry, such as the formation of $Li_{0.3}In_{1.7}$ during discharge or the transition from Li_3In_2 to Li_5In_4 during charge. Thirdly, the transition between $Li_{0.3}In_{1.7}$ and LiIn happens at 0.57 V during discharge and at 0.68 V during charge while the transition between Li_2Ga_7 and LiGa happens and 0.46 V during discharge and 0.76 V during charge. Meaning that the first one happens at a higher potential than the second during discharge but at a lower potential during charge. However, the differences in potential are quite small.

SEM analyses were performed to observe the morphology of galinstan electrodes before and after cycling. As shown in Fig. 4a, most particles of galinstan are spherical before cycling, while some larger particles have a less regular shape. The same morphology was observed after cycling (see Fig. 4b). The typical size of the particles changes from about 100 nm to 50 μm. The particle sizes are inhomogeneous in the samples before and after cycling, no trend of particle pulverization nor agglomeration can be observed (additional SEM images at lower magnification can be found in Fig. S2). EDS shows that gallium, indium and tin are dispersed homogeneously in the galinstan particles both before and after cycling. Before cycling, the composition of galinstan is 70.9 wt% Ga, 18.4 wt % In, and 10.7 wt% Sn. After cycling, the composition of galinstan is 71.3 wt% Ga, 17.4 wt% In, and 11.3 wt% Sn. The small variations

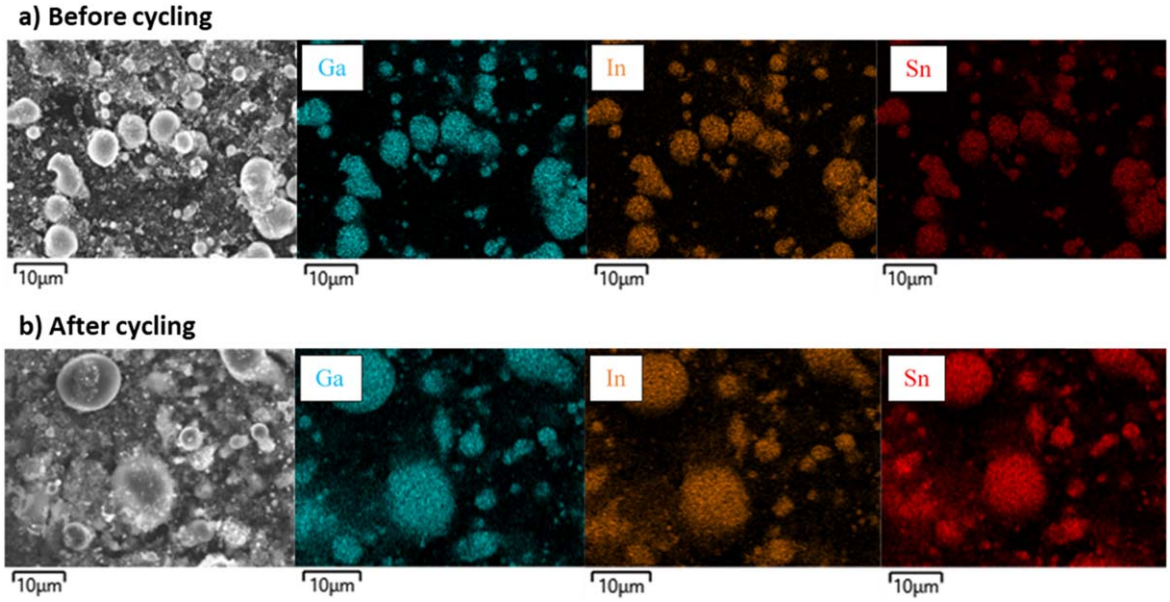

Figure 4. SEM images of the electrode powder of galinstan+C (90:10) (a) before cycling and (b) at the end of the first charge, at 1.3 V. The electrodes came from half-cells using a galinstan+C (90:10) working electrode and Li as counter and reference electrode. The electrolyte used was 1 M $LiPF_6$ in EC:DEC (1:1 volume ratio) with 5 wt% of FEC. The cells were cycled at C/20 between 0.001 and 1.3 V with a first cycle at 5 mA.

Table I. Possible phase transitions happening during the lithiation/delithiation of galinstan at the various potentials observed by cyclic voltammetry.

	Potential (V vs Li^+/Li)	Phase transition during lithiation/delithiation
Discharge	0.75	$Ga \rightarrow Li_2Ga_7$
	0.57	$Li_{0.3}In_{1.7} \rightarrow LiIn$
	0.46	$Li_2Ga_7 \rightarrow LiGa$
	0.28	$LiIn \rightarrow Li_5In_4$
	0.09	$Li_5In_4 \rightarrow Li_3In_2$
	0.001	$LiGa \rightarrow Li_2Ga$
Charge	0.42	$Li_2Ga \rightarrow LiGa$
	0.46	$Li_5In_4 \rightarrow LiIn$
	0.68	$LiIn \rightarrow Li_{0.3}In_{1.7}$
	0.76	$LiGa \rightarrow Li_2Ga_7$
	0.86	$Li_{0.3}In_{1.7} \rightarrow In$
	0.93	$Li_2Ga_7 \rightarrow Ga$

of composition could be due to a margin of error in the EDS measurements. It can be considered that there was no phase segregation, and that the composition of galinstan was homogeneous, even after cycling. The lithiation of galinstan was found to be highly reversible with SEM, but also with XRD measurements, demonstrating a return to its liquid state upon de-lithiation.

Conclusions

Galvanostatic cycling, cyclic voltammetry, XRD measurements and SEM analyses were used to study the electrochemical reactions occurring during the lithiation of galinstan and its self-healing properties. Galinstan electrodes had a practical capacity of approximately 386 mAh g^{-1}. This capacity was mainly due to the formation of LiGa and LiIn phases, as confirmed by XRD measurements. No evidence that tin participates in the electrochemical reaction could be found. An attempt to link the different potentials of reaction with the formation and decomposition of various Li_xGa and Li_xIn compounds was done but a good interpretation remains difficult due to possible overlapping of different reactions. The lithiation of galinstan was found to be highly reversible with XRD measurements demonstrating a return to its liquid state at the end of the delithiation. SEM analyses showed that the liquid alloy particles have similar morphology before and after cycling and that their composition remains homogeneous. These observations show that galinstan forms solid lithiated phases upon lithiation and returns to its liquid state after delithiation demonstrating its self-healing properties. Nevertheless, further work is needed to understand why tin does not seem to participate in the electrochemical reactions and to investigate long-term cycling stability of galinstan electrodes to know if the reversibility of the lithiation reaction could actually lead to lifetime improvements.

Acknowledgments

We acknowledge STandUP for Energy and the Erasmus+ program for the financial support, as well as Myfab Uppsala for providing facilities and experimental support. Myfab is funded by the Swedish Research Council as a national research infrastructure. The authors would like to acknowledge the financial support by the Swedish Energy Agency via project 51996–1.

ORCID

Ronan Le Ruyet https://orcid.org/0000-0002-7995-3386
Reza Younesi https://orcid.org/0000-0003-2538-8104

References

1. N. Nitta, F. Wu, J. T. Lee, and G. Yushin, *Mater. Today*, **18**, 252 (2015).
2. J. Hassoun, G. Derrien, S. Panero, and B. Scrosati, *Adv. Mater.*, **20**, 3169 (2008).
3. L. C. Loaiza, L. Monconduit, and V. Seznec, *Small*, **16**, 1905260 (2020).
4. X. Guo, L. Zhang, Y. Ding, J. B. Goodenough, and G. Yu, *Adv. Funct. Mater.*, **28**, 1804649 (2018).
5. Y. Wu, L. Huang, X. Huang, X. Guo, D. Liu, D. Zheng, X. Zhang, R. Ren, D. Qu, and J. Chen, *Energy Environ. Sci.*, **10**, 1854 (2017).
6. S. N. S. Hapuarachchi, J. Y. Nerkar, K. C. Wasalathilake, H. Chen, S. Zhang, A. P. O'Mullane, and C. Yan, *Batter. Supercaps*, **1**, 122 (2018).
7. S. N. S. Hapuarachchi et al., *ACS Appl. Energy Mater.*, **3**, 5147 (2020).
8. B. Han, Y. Yang, X. Shi, G. Zhang, L. Gong, D. Xu, H. Zeng, C. Wang, M. Gu, and Y. Deng, *Nano Energy*, **50**, 359 (2018).
9. J. Yang, J. Li, Z. Yang, J. Liu, Y. Xiang, and F. Wu, *ACS Appl. Energy Mater.*, **5**, 12945 (2022).
10. L. Lin, L. Suo, Y. S. Hu, H. Li, X. Huang, and L. Chen, *Adv. Energy Mater.*, **11**, 2003709 (2021).
11. Y. Plevachuk, V. Sklyarchuk, S. Eckert, G. Gerbeth, and R. Novakovic, *J. Chem. Eng. Data*, **59**, 757 (2014).
12. N. B. Morley, J. Burris, L. C. Cadwallader, and M. D. Nornberg, *Rev. Sci. Instrum.*, **79**, 056107 (2008).
13. D. S. Evans and A. Prince, *Met. Sci.*, **12**, 411 (1978).
14. J. Yan, Y. Lu, G. Chen, M. Yang, and Z. Gu, *Chem. Soc. Rev.*, **47**, 2518 (2018).
15. R. D. Deshpande, J. Li, Y.-T. Cheng, and M. W. Verbrugge, *J. Electrochem. Soc.*, **158**, A845 (2011).
16. Y. Lin, J. Genzer, and M. D. Dickey, *Adv. Sci.*, **7**, 2000192 (2020).
17. K. T. Lee, Y. S. Jung, T. Kim, C. H. Kim, J. H. Kim, J. Y. Kwon, and S. M. Oh, *Electrochem. Solid-State Lett.*, **11**, A21 (2008).
18. W. Yang, X. Zhang, H. Tan, D. Yang, Y. Feng, X. Rui, and Y. Yu, *J. Energy Chem.*, **55**, 557 (2021).
19. J. Saint, M. Morcrette, D. Larcher, and J. M. Tarascon, *Solid State Ion.*, **176**, 189 (2005).
20. N. Nitta and G. Yushin, *Part. Part. Syst. Charact.*, **31**, 317 (2014).
21. A. L. Santhosha, L. Medenbach, J. R. Buchheim, and P. Adelhelm, *Batter Supercaps*, **2**, 524 (2019).
22. M. Winter and J. O. Besenhard, *Electrochim. Acta*, **45**, 31 (1999).
23. F. Xin and M. S. Whittingham, *Electrochem. Energy Rev.*, **3**, 643 (2020).
24. F. Robert, P. E. Lippens, J. Olivier-fourcade, J. Jumas, and F. Gillot, *J. Solid State Chem.*, **180**, 339 (2007).
25. I. Courtney and J. Tse, *Phys. Rev. B Condens. Matter Mater. Phys.*, **58**, 15583 (1998).
26. A. R. Kamali and D. J. Fray, *Rev. Adv. Mater. Sci.*, **27**, 14 (2011).
27. Y. Huang, H. Wang, Y. Jiang, and X. Jiang, *Mater. Lett.*, **276**, 128261 (2020).
28. S. A. Webb, L. Baggetto, C. A. Bridges, and G. M. Veith, *J. Power Sources*, **248**, 1105 (2014).
29. S. D. Beattie, T. Hatchard, A. Bonakdarpour, K. C. Hewitt, and J. R. Dahn, *J. Electrochem. Soc.*, **150**, A701 (2003).
30. R. Le Ruyet, J. Kullgren, A. J. Naylor, and R. Younesi, *J. Electrochem. Soc.*, **169**, 060525 (2022).
31. J. R. Dahn, I. A. Courtney, and O. Mao, *Solid State Ion.*, **111**, 289 (1998).
32. T. Li, Y. Cui, L. Fan, X. Zhou, Y. Ren, V. De Andrade, F. De Carlo, and L. Zhu, *Appl. Mater. Today*, **21**, 100802 (2020).